Sediment Resuspension and Mixing by Resonantly Generated Internal Solitary Waves

D. BOGUCKI

Department of Aerospace Engineering, University of Southern California, Los Angeles, California

T. DICKEY

Ocean Physics Laboratory, University of California, Santa Barbara, Santa Barbara, California

L. G. REDEKOPP

Department of Aerospace Engineering, University of Southern California, Los Angeles, California

(Manuscript received 8 May 1995, in final form 1 January 1996)

ABSTRACT

The observation of internal solitary waves (ISWs) propagating upstream along a strongly stratified bottom layer on the California shelf is reported. An increased concentration of particulates in the water column accompanies the passage of these ISW packets. The estimated local Richardson number in the bottom vicinity is around 1/4, and a vertical coefficient of eddy diffusivity of order 10^{-2} m^2 s^{-1} is associated with the upstream propagating leading ISW. The leading ISW gave rise to reversed flow in an 8-m layer above the bottom. It is argued that the upstream propagating ISWs were generated by resonant flow over bottom topography. Internal waves generated in this way seem to be frequent in the record of a month-long experiment. Model results suggest that the ISWs can carry up to 73% of such generated long wave energy. The ocean conditions at the site are similar to those of other coastal sites, which suggests that the phenomenon described here may be common.

1. Introduction

Internal solitary waves (ISWs) are waves of permanent form propagating in a shallow, stratified layer and are maintained by the balance between the nonlinear effects of steepening and linear dispersion. They have been observed on the continental shelf (Ostrovsky and Stepanyants 1989), where the water column consists of a thin stratified upper-layer overlaying a thicker well-mixed lower layer. On the California shelf, observations of ISWs have been documented by Howell and Brown (1985). It has been suggested that ISW-induced mixing and transport (Bogucki and Garrett 1993) are usually confined to the upper stratified part of the water column. The role of ISW-induced mixing and resuspension of bottom sediments is not known because there have been few reported observations of ISWs that propagate close to the ocean bottom. Intermittent energetic mixing events at the bottom boundary layer are expected to redistribute sediments, heat, or chemical substances, such as nutrients or pollutants (Garrett 1979). This becomes increasingly important in the shallow coastal zone where enhanced stirring affects a major portion of the water column. Our experiment site, the shelf bottom off Palos Verdes peninsula in the Los Angeles area, has been declared ''the nation's largest ocean dumping ground of DDT'' (*Los Angeles Times*, September 10, 1992). It is estimated that 200 tons of DDT remain in sediment layers in this area (Nichols and Young 1991). This situation reinforces the importance of resuspension and mixing processes at the present site. However, similar waste sites are common to other population centers.

Here we report the observation of ISW packets propagating along a strongly stratified bottom layer on the California shelf and a strong concurrent increase in suspended particulate matter in the water column. Sediment resuspension is traditionally expected to occur when the current speed in the outer part of the boundary layer increases above a threshold value (e.g., Grant and Madsen 1986), giving rise to a strong shear stress acting on the bottom surface. However, our observation of a selected ISW event (day 42) coincides with a marked increase in the concentration of suspended particulates even though the near-bottom current speed was low and close to a minimum. This situation is not unique. In fact, several studies (Churchill et al. 1987, 1994; Cacchione et al. 1994) have previously noted events of elevated beam attenuation (indicative of high

Corresponding author address: Dr. D. Bogucki, Department of Aerospace Engineering, University of Southern California, Los Angeles, CA 90089-1191.
E-mail: DBogucki@Earth.usc.edu

particulate concentrations), which occur during low bottom stress conditions (up to 70% of the observed events). This anomalous effect has sometimes been attributed to bottom dredging by trawlers (Churchill et al. 1994).

It is postulated here that ISW-induced resuspension and successive mixing may explain the occurrence of a relatively rapid (with respect to the background stratification) increase in particulate matter during low bottom current speeds. For two-layer flow (upper well mixed/lower stratified) and in the absence of background shear, the largest ISW-induced shear occurs at the top of the stratified layer (Bogucki and Garrett 1993). This relationship changes for ISWs propagating upstream on the shear flow. As the mean shear of the flow increases (for constant ISW amplitude) the zone of maximum ISW-induced shear is pushed downward toward the bottom. This, together with the ISW-induced unsteady flow in the bottom boundary layer, can potentially result in resuspension/mixing.

The aim of this paper is to discuss the role ISWs may play in near-bottom vertical mixing and sediment resuspension and to propose a mechanism for the generation of a class of ISWs that are candidates for creating a dynamical field favorable for resuspension. This paper is organized as follows: First, we describe the background conditions during the experiment. Then we present a theory of long internal waves in a sheared environment. We go on to discuss how the observed phenomenon has the features of an ISW propagating on a thin stratified bottom layer against the current. Next we show evidence of increased sediment resuspension and possible mixing by the leading ISW and suggest a mechanism by which the ISWs can resuspend sediment and generate/enhance vertical mixing. We then propose that the observed ISWs were generated by the resonant interaction of the current with the bottom topography and show results from numerical simulations of transcritical flow over bottom topography. Finally, the implications of ISWs for coastal bottom resuspension/mixing processes are discussed.

2. The experiment

The experiment was conducted on the Southern California shelf in spring 1992, between yearday 9 and yearday 48 (January 9–February 17) (Dickey et al. 1993). An interesting series of internal wave events were observed throughout this period. The focus of the present study is primarily on one internal wave packet, recorded on day 42. For the experiment, a mooring was placed near the shelf break 60-m isobath approximately 2 km offshore of the Palos Verdes Peninsula. Additionally, vertical hydrographic profiles of the water column were taken on days 15, 16, and 33. Multivariable moored systems (MVMS) were placed on the mooring at 8, 12, 30, and 50 m above the bottom (hereafter denoted as mab). The mooring location and the shelf bottom topography are shown in Figs. 1 and 2, respectively.

Each MVMS recorded horizontal currents, temperature, and beam attenuation coefficient (referred to herein as b.c.), which is a measure of water turbidity. The unit at 30 mab also measured conductivity. The sensor packages sampled these physical and optical parameters every minute for 39 days. At the bottom, a piezoelectric sensor measured pressure every second.

The value of b.c. gives an instantaneous measure of water turbidity. In near-bottom water, b.c. tends to correlate well with the concentration of particulate matter in an approximately linear relationship (Spinrad et al. 1989). In our experiment, the absolute values of b.c. after day 22 are affected by biofouling, so we concentrate on the short-term variability by high-pass filtering the b.c. record.

The current velocity measurements were averaged over 1 minute. The temperature sensor mounted in the MVMS has a relatively ''slow'' time constant ($\sim$100 s) (Levine 1981), thus temperature records are effectively the result of convolving the temperature signal data with a 100-s time-averaging window.

Oceanographic conditions

The background stratification of the water column during the experiment is characterized by a stratified bottom layer and a well-mixed upper layer. Density profiles on days 16 and 33 show the thermocline at 10 to 20 mab (see Fig. 3). This is consistent with long-term observations (Hickey 1992) where along the 15-yr seasonally averaged cross-shelf transect, the isopycnals are characteristically tilted: At 1000 km offshore, the thermocline depth is around 150 m, while near the shore the thermocline is shallower than 50 m. The angle of tilt is related to the mean geostrophic alongshore current and is a dominant feature of the density structure in spring. A detailed explanation for the existence and dynamics of this stratified near-bottom layer is presented in Hickey (1992).

The stratification profile of the water column at the experiment site can thus be well approximated by a piecewise constant value of the Brunt–Väisälä frequency $N(z)$ in each layer. The value of N in the stratified bottom layer is approximately 10^{-2} rad s^{-1} with a corresponding buoyancy oscillation period of about 8 min. During the experiment $N(z)$ was measured only three times; the last time was 9 days prior to the primary ISW observations. Thus, the $N(z)$ corresponding to the ISW passage must be inferred. The observed vertical extent of the stratified layer in the CTD casts varies in time (Fig. 3). The strength of the density gradient in the stratified layer was proportional to the temperature difference across a 4-m interval (centered at 10 mab) recorded by the mooring (Fig. 3). This density gradient fluctuates throughout the experiment, but was within a factor of 0.2 on day 33 and day 42, during ISW passage.

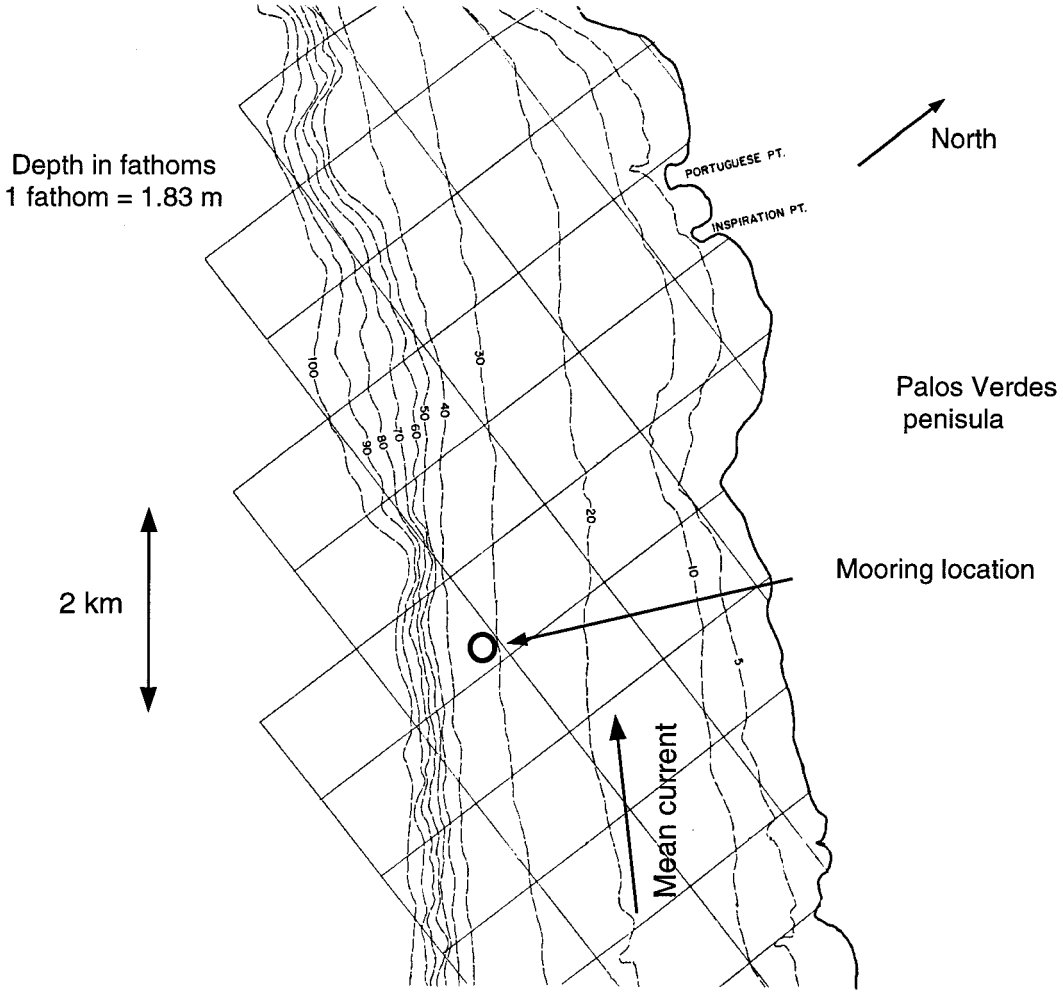

FIG. 1. Mooring location off the Palos Verdes Peninsula.

Thus, we use the last measured density profile for our calculations.

Another important parameter is the background current speed $U(z)$. During our experiment the observed mean current corresponds to typical spring conditions (Hickey 1992): the poleward California Countercurrent is the dominant feature with speeds $O(10\ \text{cm s}^{-1})$ at the surface and $O(1\ \text{cm s}^{-1})$ near the bottom. The vertical current structure at the experimental site also depends on local conditions. In particular, the principal ISWs were observed toward the end of a storm. At that time, a relatively constant wind stress over 3 days created an upwelling circulation at the mooring site and a reinforced poleward component of subsurface currents up to 30 cm s^{-1}. The associated vertical shear components, du/dz (alongshore) and dv/dz (cross shore) are of order $5 \times 10^{-3}\ \text{s}^{-1}$ based on profiles shown in Fig. 4.

Throughout the experimental period, events of similar character were frequently observed. About 10 events in the data record were noted in which high b.c. values were accompanied by pulses in the temperature and current meter record corresponding to the passage of a large internal wave. Two examples are shown in Fig. 5. Estimates of the limiting longwave speeds for the measured current and stratification suggest that the b.c. peak coincides with the time when the local Froude number is near unity (i.e., the current speed at 12 mab is then about 10 cm/s). The ISW wave train selected for analysis in this paper is the only one in which we clearly observe the rank-oriented waves at the mooring location, characteristic of a fully dispersed ISW wave train and large enough to be present in the record of at least two neighboring current meters. In general, a dedicated experiment is needed to capture such events. The ISW wave packet selected for analysis in this paper is shown in Fig. 6 with another vigorous event. The event we analyze in most detail is shown in Fig. 6 (panel A2), where the selected leading internal wave has a period of 11 min, comparable to the background Brunt–Väisälä period. Waves of that frequency propagate horizontally and are long internal waves.

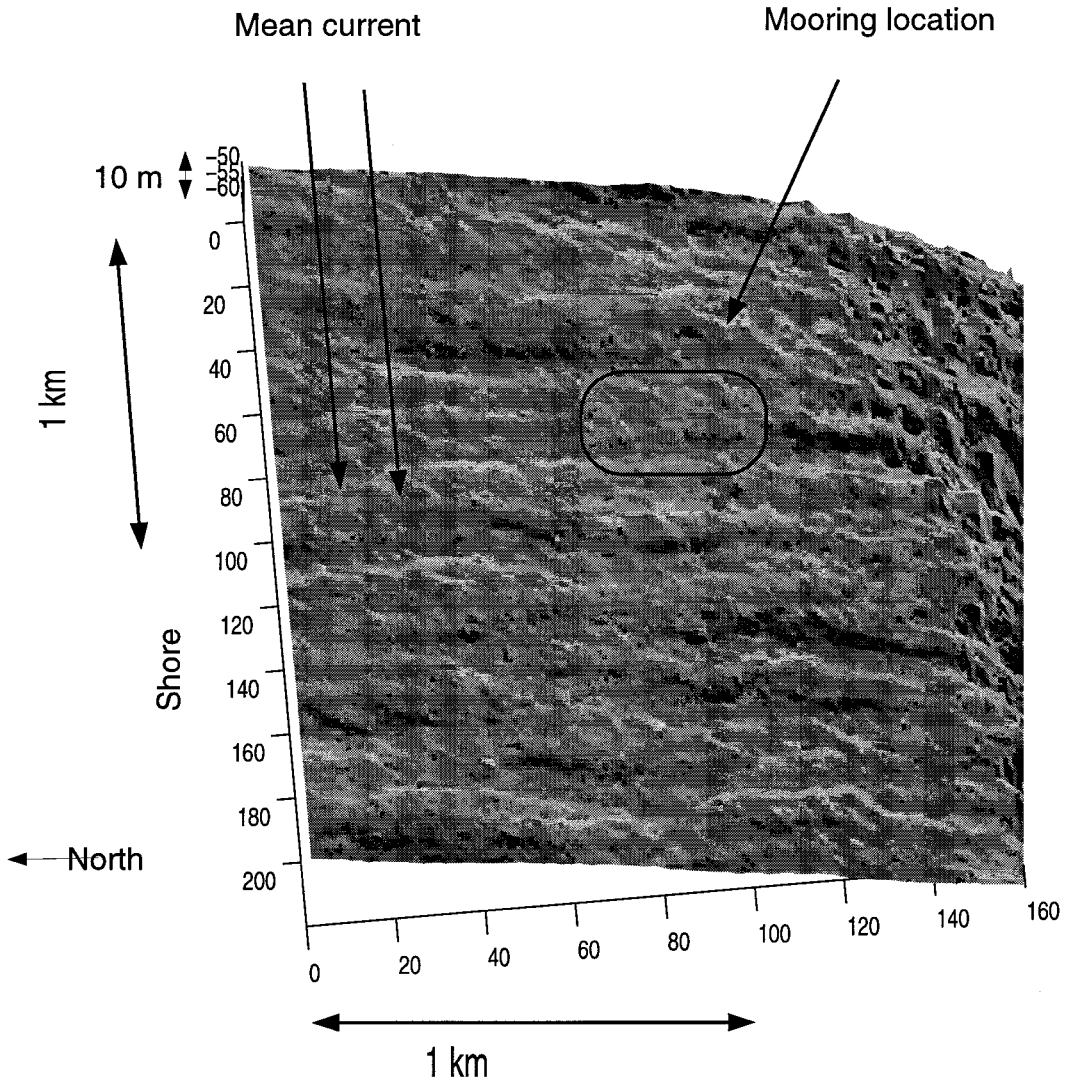

FIG. 2. Bottom topography (courtesy of USGS) and the approximate mooring location.

3. Theory

The properties of long linear internal waves in a general waveguide are given by the Taylor–Goldstein equation

$$\phi'' - \frac{U''}{(U-c)}\phi + \frac{N^2}{(U-c)^2}\phi = 0, \qquad \phi(0) = \phi(h) = 0. \tag{1}$$

This equation determines the phase speed c (eigenvalue) and modal amplitude ϕ (eigenfunction) for inviscid, long internal wave modes where the mean flow, $U(z)$, has velocity shear. All velocities are measured relative to the stationary bottom boundary. The eigenfunction $\phi(z)$ is directly proportional to the vertical velocity and its gradient yields the perturbation horizontal velocity relative to $U(z)$. In the present case, the profile of the Brunt–Väisälä frequency $N(z)$ and the velocity $U(z)$ are approximated by the following functions of the distance from the bottom:

$$N(z) = \begin{cases} N_1, & 0 < z < d \\ 0, & d < z < h \end{cases} \tag{2}$$

$$U(z) = \begin{cases} U_0 + \gamma_1 z, & 0 < z < d \\ U_0 + \gamma_1 d + \gamma_2 (z-d), & d < z < h. \end{cases} \tag{3}$$

This two-layer model was selected because it represents both a reasonable approximation of the local environment as measured during the present experiment (shown in Figs. 3 and 4) and it permits analytical solutions of the eigenvalue problem (1).

Using the given Brunt–Väisälä and constant shear velocity profiles, the long wave limit of the Taylor–Goldstein equation can be expressed in the form

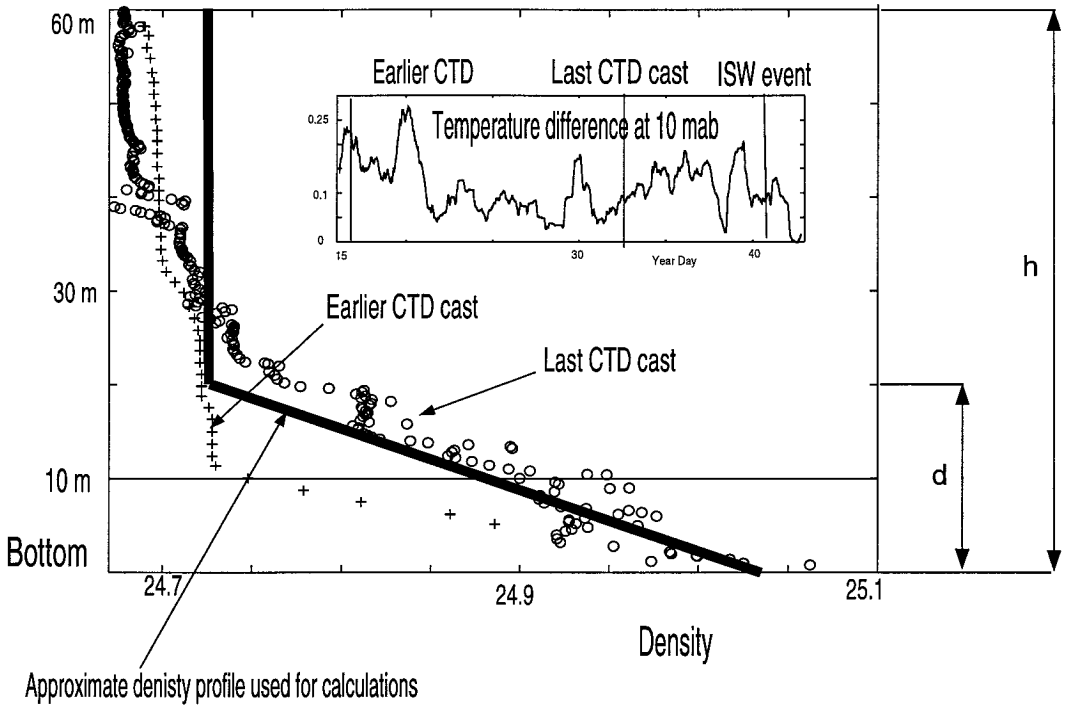

FIG. 3. Density profiles from the CTD casts 16 and 9 days prior to ISW passage and time series of temperature difference across a 4-m vertical interval centered at 10 mab.

$$\phi'' = \begin{cases} -\dfrac{J_1}{(z - \tilde{c})^2}\phi, & 0 < z < d \\ 0, & d < z < h, \end{cases} \tag{4}$$

where J_1 is the alongshore component of the Richardson number $(N_1/\gamma_1)^2$ ($\gamma_1 = du/dz$) of the lower, stratified layer and $\tilde{c}$ is a rescaled measure of the phase speed, with the units of length, defined by

$$\tilde{c} = \frac{(c - U_0)}{\gamma_1}. \tag{5}$$

The solutions in each layer satisfying the (homogeneous) boundary conditions of vanishing normal velocity at the bottom and top of the water column are

$$\phi(z) = \begin{cases} B|z - \tilde{c}|^{1/2} \cos(\mu_1 \ln|z - \tilde{c}| - \Delta), & 0 < d < z \\ -B\gamma_1 \dfrac{(d - \tilde{c})}{(h - d)}(h - z), & d < z < h, \end{cases} \tag{6}$$

where the parameter B is an arbitrary scaling parameter and

$$\mu_1 = \left(J_1 - \frac{1}{4}\right)^{1/2}$$

$$\Delta = \mu_1 \ln|\tilde{c}| - \pi/2.$$

For the assumed inviscid flow, the solution in the two adjacent layers must satisfy continuity of vertical particle velocity and of the normal stress (i.e., pressure) at their common interface. In the linearized limit, the matching conditions where the mean velocity is continuous across the interface can be written, respectively, as

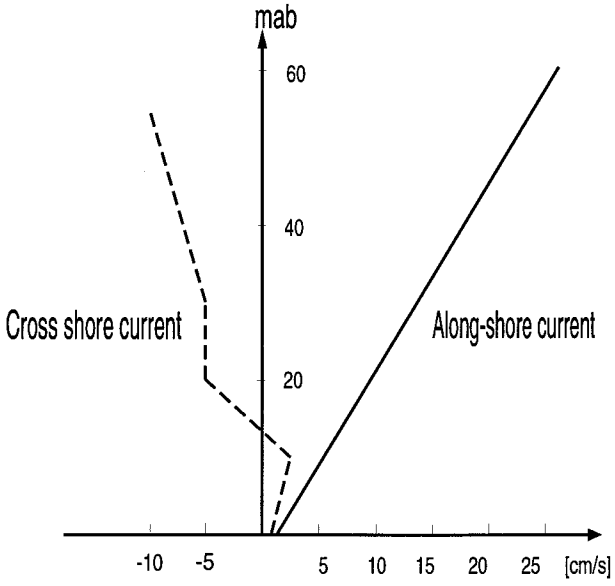

FIG. 4. Alongshore velocity component $u(z)$ and cross-shore $v(z)$. They represent 10-min averaged values, calculated prior to the leading ISW passage.

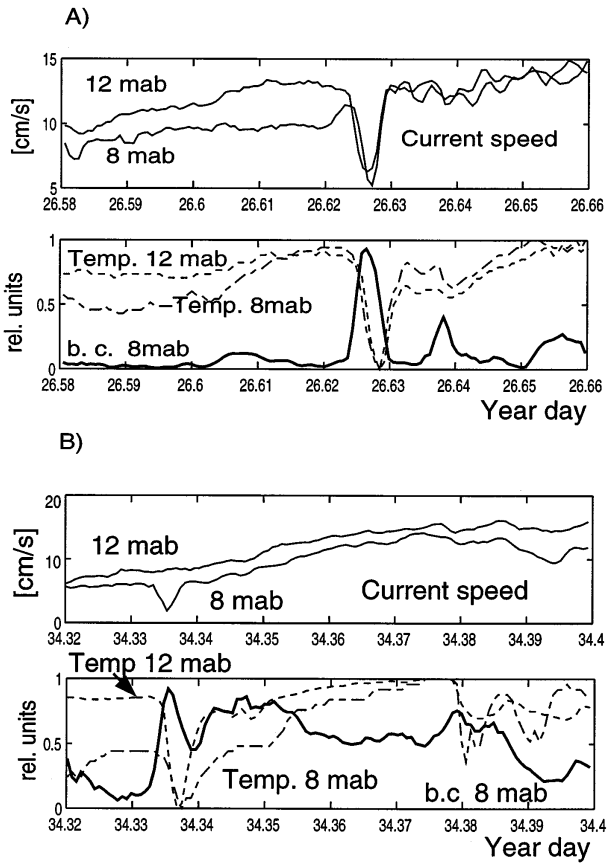

FIG. 5. Observed internal wave events: b.c., temperature, and current velocity time series.

$$\left[\left|\phi\right|\right] = 0 \tag{7}$$

$$\left[\left|U'\phi - (U - c)\phi\right|\right] = 0, \tag{8}$$

where $[|\cdots|]$ denotes the jump in the indicated quantity across the interfacial boundary located at its equilibrium position $z = d$. Application of these matching conditions using the solutions (6) yields the eigenvalue relation for $\tilde{c}$, which we express in the form

$$\tan\theta_d \equiv \tan\left(\mu_1 \ln\left|\frac{d - \tilde{c}}{\tilde{c}}\right| + \frac{\pi}{2}\right) = \Gamma$$
$$\equiv \frac{(2\gamma_2 - \gamma_1)(h - d) + 2\gamma_1(d - \tilde{c})}{2\mu_1\gamma_1(h - d)}. \tag{9}$$

This relation can be written in the alternate form

$$\tilde{c} = \frac{d}{1 \pm E}, \tag{10a}$$

where E is defined as

$$E = \exp\left\{\frac{1}{\mu_1}\left[\tan^{-1}\Gamma + \left(n + \frac{1}{2}\right)\pi\right]\right\},$$
$$n = 0, \pm 1, \pm 2, \cdots. \tag{10b}$$

Although (10a) is still an implicit solution for $\tilde{c}$ since the eigenvalue also appears in the expression for Γ, it serves to help classify the types of modes and is useful for computational purposes. Values of $\tilde{c}$ computed using the plus sign in the denominator of (10a) correspond to internal wave modes where $\tilde{c} < 0$ or $\tilde{c} > d$. Values of $\tilde{c}$ obtained by use of the negative sign are critical layer modes where $0 < \tilde{c} < d$ so that (4) is singular at $z = \tilde{c}$. These modes are inviscid singular neutral modes of the Taylor–Goldstein equation and exist only for $J_1 > 1/4$. They require the insertion of an inner solution, a nonlinear critical layer whose thickness scales with the two-thirds power of the wave amplitude, centered around the critical level $z = \tilde{c}$ to yield a nonsingular modal amplitude function (Maslowe and Redekopp 1980).

Korteweg–de Vries theory

When long waves have significant amplitude (compared to the depth of the stratified layer along which they are ducted), then (weak) nonlinearity should be important to their dynamics. Of course, we know that nonlinearity will always become important at some point along a linear characteristic when the system is weakly dispersive and dissipative effects are ignored. For this reason, the weakly nonlinear theory leading to the Korteweg–deVries equation is reviewed for the free evolution of a wave packet propagating along a characteristic of the linear system in the long wave limit. Coefficients of the leading nonlinear and dispersive terms for a realistic model of the observed mean flow are presented.

The Boussinesq equations of motion for plane wave disturbances relative to a mean shear flow $U(z)$ of a hydrostatically balanced state with Brunt–Väisälä frequency $N(z)$ are taken in the form

$$u_t + Uu_x + wU' + uu_x + wu_z = -p_x \tag{11}$$

$$w_t + Uw_z + uw_x + ww_z = -p_z - \sigma \tag{12}$$

$$\sigma_t + U\sigma_x - wN^2 + \sigma_x + w\sigma_z = 0 \tag{13}$$

$$u_x + w_z = 0. \tag{14}$$

These equations, and the results that follow, are all presented in dimensional form. In the above equations p is the pressure (scaled by the mean density) relative to the hydrostatic value, σ is the perturbation buoyancy, and u and w the perturbation velocity components. For long waves along a single characteristic and for a given internal wave mode, these equations admit an asymptotic expansion for the disturbance fields of the form

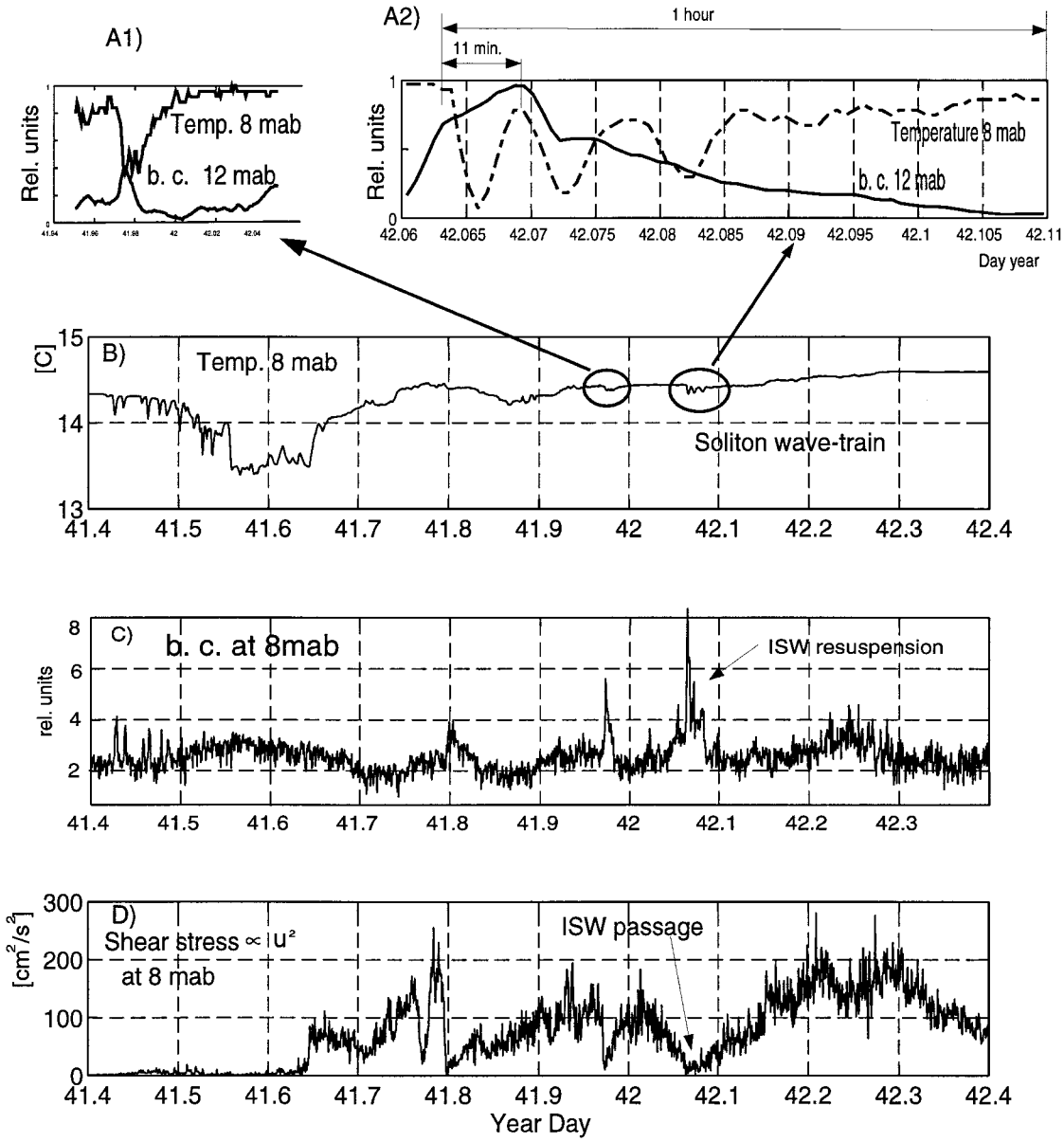

FIG. 6. Analyzed soliton wave train (a2) and another internal wave train event 2 hours earlier (a1); (b) temperature at 8 mab; (c) b.c. at 8 mab; (d) shear stress (which is proportional to u^2) at 8 mab.

$$u(x, z, t) = A(x, t)\phi'(z) + \frac{1}{2}A^2\phi_n'(z) + A_{xx}\phi_d'(z) + \cdots \quad (15)$$

$$w(x, z, t) = -A_x\phi(z) - AA_x\phi_n(z) - A_{xxx}\phi_d(z) + \cdots \quad (16)$$

$$p(x, z, t) = A\{U'\phi - (U - c)\phi'\} + \frac{1}{2}A^2p_n(z) + A_{xx}p_d(z) + \cdots \quad (17)$$

$$\sigma(x, z, t) = -A\frac{N^2\phi}{U - c} + \frac{1}{2}A^2\sigma_n(z) + A_{xx}\sigma_d(z) + \cdots, \quad (18)$$

provided the amplitude function $A(x, t)$ evolves according to the law

$$A_t = -cA_x + \alpha AA_x + \beta A_{xxx} + \cdots. \quad (19)$$

The linear eigenfunction $\phi(z)$ is a solution of the long wave limit of the Taylor–Goldstein equation (1) with eigenvalue c. The coefficients α and β in (19) emerge,

respectively, from solvability conditions for the higher-order terms in the expansions (15)–(18). For the specific flow model discussed earlier and given by (2) and (3), these coefficients are defined by

$$\alpha = \frac{\gamma_1}{\mathcal{D}(d-\tilde{c})}\left\{2J_1 + \frac{1}{4} + 3\mu_1\Gamma\frac{\gamma_2-\gamma_1}{\gamma_1} - \left(\frac{2\gamma_2-\gamma_1}{2\gamma_1}\right)^2 + \frac{\gamma_2-\gamma_1}{2\gamma_1} + \frac{1}{J_1+2}\left[(2J_1+1)\left(\mu_1\Gamma - \frac{3}{4}\right) + 2(\mu_1\Gamma)^3 - 2\mu_1^2(1+\Gamma^2)\right] - (-1)^n\frac{2\mu_1^3(1+\Gamma^2)^{3/2}}{J_1+2}\left|\frac{d-\tilde{c}}{\tilde{c}}\right|^{3/2}\right\}; \tag{20}$$

$$\beta = \frac{\gamma}{\mathcal{D}}\left\{\frac{1}{3}(d-\tilde{c})(h-d) - \frac{\mu_1^2(1+\Gamma^2)}{4J_1+3}[\tilde{c}^2 - (d-\tilde{c})]^2 + \frac{2(1+\mu_1\Gamma)}{4J_1+3}(d-\tilde{c})^2\right\}, \tag{21}$$

where

$$\mathcal{D} = \frac{1}{h-d}\left\{1 - \mu_1^2(1+\Gamma^2)\frac{d(h-d)}{\tilde{c}(d-\tilde{c})}\right\}. \tag{22}$$

The scaled phase speed $\tilde{c}$ defined in (5) is obtained from the eigenvalue condition given by (9), and the parameter n corresponds to the mode number as specified in (10b).

4. Soliton observations and properties

The internal wave train chosen for analysis consists of three solitary waves (panel A2 of Fig. 6). The soliton wave train signature is seen here as a series of troughs in the temperature record (panels a and b of Fig. 6). The amplitude of the leading observed wave was taken to be the maximum observed isotherm displacement at 8 mab. This value is 4 m (Fig. 7) and is an underestimate of the leading wave amplitude since the sensor location does not correspond to the location of the maximum isopycnal displacement and the large thermal inertia of the sensor leads to significant temporal averaging. The leading wave, which is also the largest, coincides with a rapid increase of the particulate load as indicated by the measurement of b.c. (panels a and c of Fig. 6).

We determined the modal function and wavelength associated with the observed ISW by analyzing the horizontal water parcel displacement vectors induced by the leading wave during its passage. These displacement vectors are derived from current meter data by first extracting the mean current a few minutes prior to wave passage. The residual displacement vectors are considered to be ISW induced. At 8 and 12 mab the displacements are in the current direction and are approximately 20 and 10 m, respectively. Farther above the bottom (at 30 and 50 mab) the water parcel displacement vectors are against the current and are approximately 12 and 7 m (Fig. 8). The displacement $\Delta s(z)$ can be expressed in terms of the modal function $\phi(z)$ (Bogucki and Garrett 1993); here z is the depth of the undisturbed streamline. Calculations of vector displacement in terms of undisturbed streamline location differ from our Eulerian measurements with an error of $O(a/d = 0.2)$, where a is the leading soliton amplitude.

The value of $\Delta s(z)$ is an exact displacement vector length for Lagrangian measurements—when following an isopycnal. The Eulerian vector displacements can be obtained with required accuracy by integrating the Eulerian series expansion of $u(x, z, t)$ as given by (15). With the background current removed, the Lagrangian displacement is

$$\Delta s(z) = \int_{-\infty}^{\infty} \frac{a\phi'(z)f(\zeta)}{1 + a\phi'(z)f(\zeta)}\, d\zeta, \tag{23}$$

where $f(\zeta) = \text{sech}^2(x - c_{\text{ISW}}t)$ is the scaled isopycnal displacement for an isolated solitary wave (c_{ISW}: soliton speed with respect to the bottom). In the first-order approximation, the expression for the ISW-induced water parcel displacement becomes

$$\Delta s(z) = aL\cdot\phi'(z) + O(a/d), \tag{24}$$

where L is the ISW length at half amplitude and is independent of ISW speed.

After fitting these displacements to the observed values it was found that the ISW length was 90 m with a relative error of 0.2. We also found that the wave was propagating *upstream* nearly parallel to the shore as indicated by the largest displacement value at 8 mab,

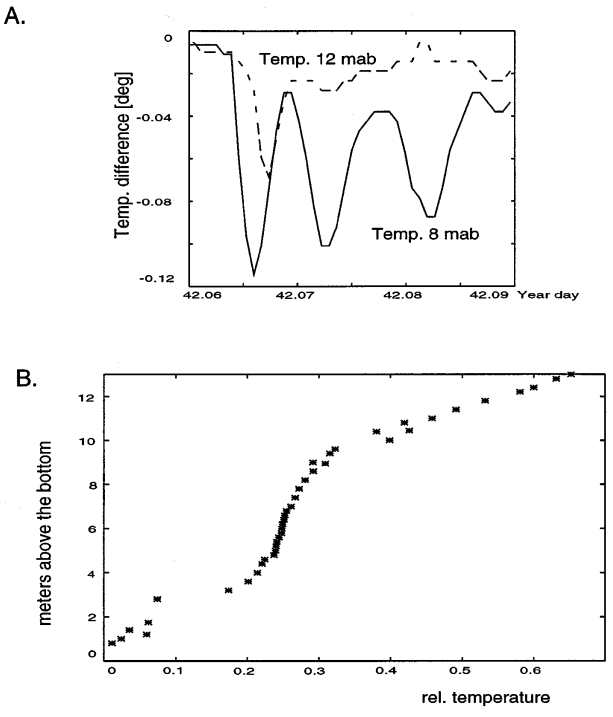

FIG. 7. The leading ISW amplitude estimate. (a) Temperature variations due to passing ISW at 8 mab; (b) relative temperature vs distance above the bottom. (Vertical hydrographic profiles were kindly provided by Dr. Libe Washburn and Dr. Burt Jones.) From panels a and b we estimated the ISW amplitude at 8 mab to be 4 m.

and the wave was of the *gravest* mode. The direction and length of the displacement vectors become less reliable farther from the bottom because the mean current increases closer to the free surface.

The linear wave speed can be estimated from (9). As a value of the residual bottom current we use $U_0 = O(1$ cm s$^{-1})$; that is, the mean geostrophic current value for that depth (Hickey 1992). A more accurate analysis, which would not require the residual bottom current, is possible by applying a WKB analysis of the Sturm–Liouville problem (1) (Bender and Orszag 1978) with $c = 0$, $U_0 = 0$, and $\gamma_1 \neq 0$. Our measurements do not warrant such accuracy and for simplicity we use a value $U_0 = O(1$ cm s$^{-1})$.

In turn, the ISW speed, c_{ISW}, depends on the wave amplitude a and the linear wave speed according to $c_{\mathrm{ISW}}/c = (1 + |\alpha|a/3)$ (Maslowe and Redekopp 1980), where α is the coefficient of the leading nonlinear term [cf. (20)]. In our case c_{ISW} is larger by a factor of 1.4 than the corresponding linear long wave eigenspeed c. Due to uncertainty in the vertical profiles of $N(z)$ and $U(z)$, the resulting value of the gravest mode internal wave speed, with respect to the bottom, is then taken as 5 cm s^{-1} with possible values ranging between 2 and 9 cm s^{-1}, obtained from (9) with different plausible $N(z)$ and $U(z)$.

The parameters of the observed leading ISW are as follows: the length is 90 m; the speed with respect to the bottom is 7 cm s^{-1}, and the amplitude 4 m. These values are used to quantify the inferred vertical current structure in the vicinity of the bottom.

a. ISW-induced Richardson number

From continuity considerations the horizontal current $u_i(x, z, t)$ induced by the passing ISW relative to the bottom is

$$u_i(x, z, t) = \frac{c_{\mathrm{ISW}} a\phi'(z) f(\zeta) - U(z)}{1 + a\phi'(z)\cdot f(\zeta)}, \qquad (25)$$

where $f(\zeta) = \mathrm{sech}^2(x - c_{\mathrm{ISW}}t)$, z is the location of the undisturbed streamline, and $U(z)$ is the mean background current. In the leading approximation,

$$u_i(x, z, t) = c_{\mathrm{ISW}} a\phi'(z) f(\zeta) - U(z) + O(a/d). \qquad (26)$$

This approximation leads to the prediction that a layer near the bottom (at most about 8 mab) under the footprint of the upstream propagating wave separates from the boundary (Fig. 9). The results of these calculations are consistent with our observations in which the alongshelf current velocity at 8 mab decreased to negligible values during ISW passage (Fig. 6). To estimate how the stability of the water column is affected by the passing ISW, we calculated the vertical distribution of the Richardson number Ri(z). The horizontal velocity induced by an ISW in the coordinate system following the ISW, $u_{\mathrm{followingISW}}$, is given by Bogucki and Garrett (1993):

$$u_{\mathrm{following\,ISW}}(\zeta, z) = -\frac{c_{\mathrm{ISW}} + U(z)}{1 + a\phi'(z)\cdot f(\zeta)}, \qquad (27)$$

and, allowing for the stretching of the stratification, the associated Richardson number at the wave crest is given by

$$\mathrm{Ri}(z) = \frac{N_0^2(1 - \eta')^5}{((U(z) + c_{\mathrm{ISW}})\eta'' - U'(z)(1 - \eta'))^2}, \qquad (28)$$

where N_0 is the undisturbed Brunt–Väisälä frequency, $\eta(z) = a\phi(z)$, and the differentiation is with respect to depth z.

These calculations show that the ISW-generated shear is largest in the lower part of the stratified water column (4–15 mab), with an associated wave-induced Richardson number of $O(1/4)$. Within the measurement error, this value might even be lower than the critical value of 1/4. It is remarkable that a relatively small ISW (the ratio of a/d is 0.2) was able to lower the Ri to near its critical value. For comparison, an ISW in a nonsheared environment must have an amplitude of 15 m (a/d is 0.75) to attain the same Ri, and its minimum Ri will coincide with the top of the stratified part of the water column. This result shows that the weakly nonlinear theory of ISWs (Maslowe and Redekopp 1980) is a valid tool to describe ISWs in sheared regimes where mixing is likely. The vertical distribution of Ri(z), modal func-

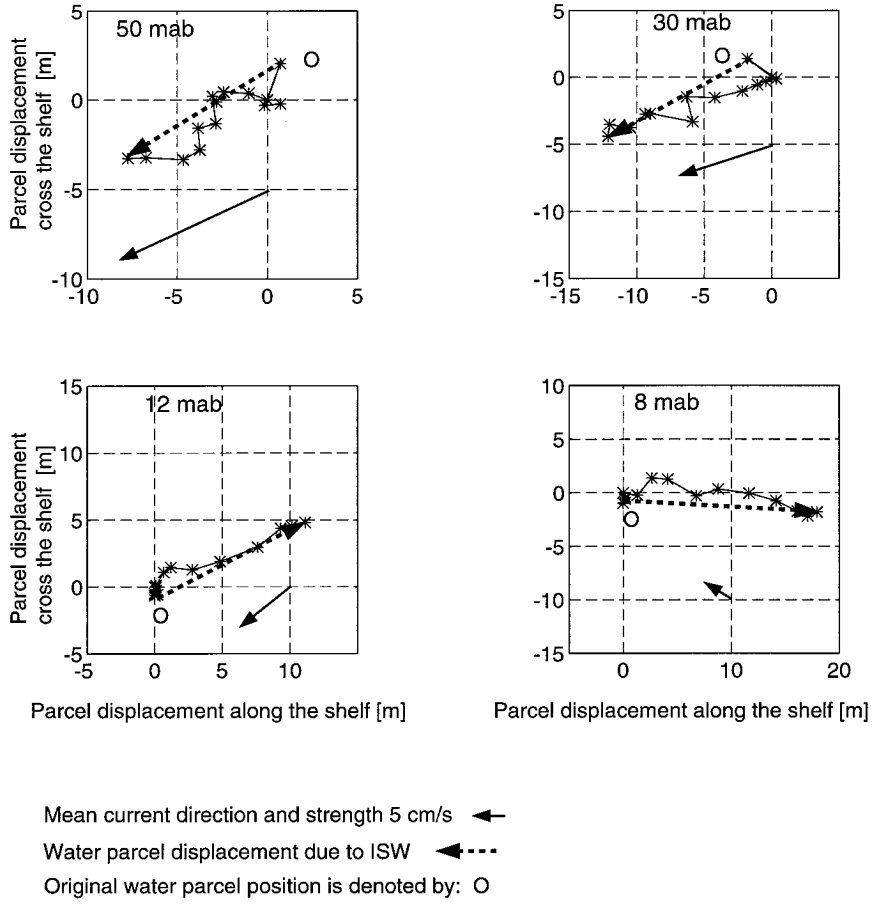

FIG. 8. Vector displacements due to the ISW and the mean current speed and direction prior to the ISW passage.

tion and wave-induced current speed versus background current, and the extension of the separation layer, are shown in Figs. 9 and 10, together with the position of the mooring sensors. The effect of ISW passage on the value of b.c. during ISW passage is shown in Fig. 6. The observed increase in b.c. at 8 or 12 mab is so large that it can be accounted for only by a new input of particles, either by advection or resuspension. Since this high particulate loading occurs near the base of the stratified bottom layer, the most likely explanation is resuspension from the bottom. In addition, the temperature–salinity diagram obtained before, during, and after ISW passage confirms that variability in temperature and salinity are negligible and that the water masses are of similar origin. In the next section we investigate the mechanism for the b.c. increase, which is one of the largest in the observed month-long record.

b. Resuspension and mixing due to the ISW

The maximum value of b.c. at 12 mab is observed 2 to 6 minutes after the b.c. at 8 mab achieves its maximum value. From (26) and observations, the vertical extent of the flow separation lies in the vicinity of the lowest sensor (i.e., less than 8 mab). Direct evidence for mixing by an ISW can be seen in Fig. 6, panel a2: the b.c. increases concurrently with the ISW passage and returns to its initial value after 1 h, long after the leading ISW is gone. This delay is presumably due to the slow rate of particle settling. The associated vertical eddy diffusivity coefficient can be estimated from the b.c. observations by using the b.c. signal as a passive tracer. The observed rapid increase in the b.c. during the wave passage can be attributed to both isopycnal displacement and ISW-induced mixing. The vertical diffusivity associated with ISW passage is inferred from the time lag between the observed maximum value of the b.c. at 8 and 12 mab using $K_V = O((\delta z)^2/\delta t)$, where δz is the vertical sensor separation and δt is the lag between observed maximum values of the b.c. at those two depths. The inferred diffusivity is $K_V = O(10^{-2})$ m^2 s^{-1}, which is two orders of magnitude larger than the typical value for mixing at boundaries estimated for this area (Ledwell and Hickey 1995) and the observed diffusivity associated with internal wave reflection and breaking on a sloping boundary (Eriksen 1994). It is

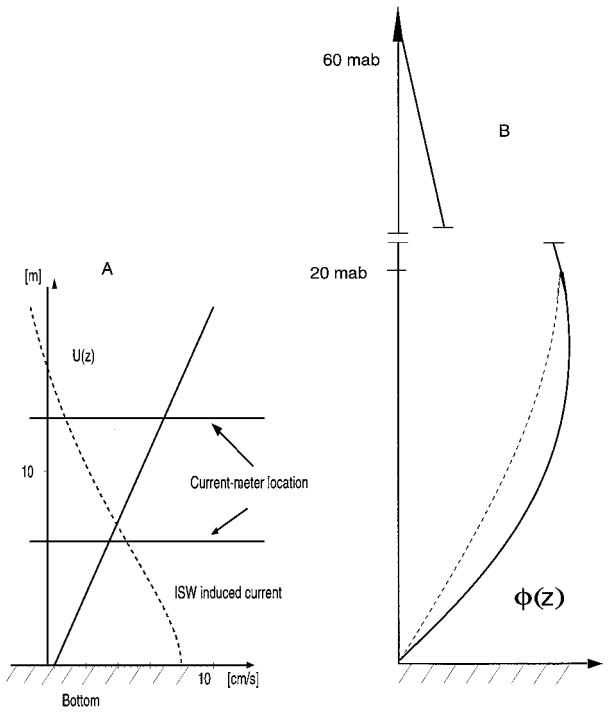

FIG. 9. (a) ISW-induced current and the background current estimated from (26). The flow is reversed in a layer 8 m deep above the bottom—the maximum ISW-induced current matches background current in opposite direction. (b) Eigenfunction associated with observed ISW and for comparison eigenfunction with no shear (broken line).

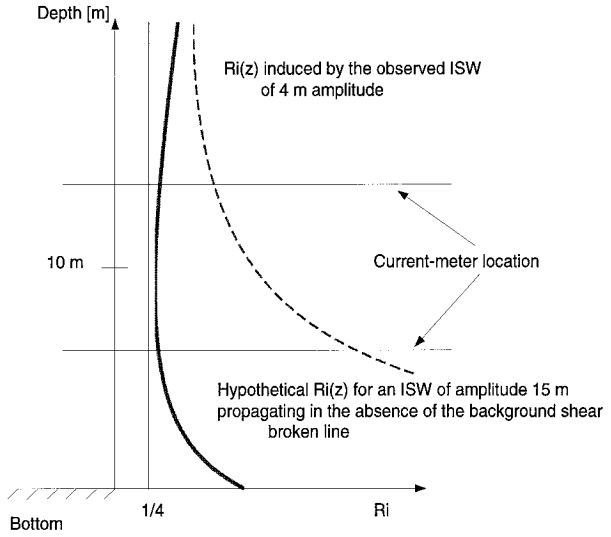

FIG. 10. Richardson number due to the combined action of background shear and the passing ISW as estimated from (28). The zone of low Richardson number and the position of the mooring sensors are also shown.

also postulated in Ledwell and Hickey (1995), on the basis of their tracer experiment (their experiment area overlaps with our mooring location—but at a different time), that the enhanced boundary mixing dominates diapycnal fluxes in the Santa Monica and San Pedro Basins.

5. Resonant generation of observed ISW

An hour prior to the ISW arrival (Fig. 11), the flow within the bottom-most layer was supercritical. That is, the Froude number $\mathrm{Fr} = U/c$, where U is some average current speed and c is the long wave speed, exceeds the critical value of unity. During wave passage, the Froude number decreased to subcritical values, $\mathrm{Fr} \leq 1$ (Fig. 11). Experiments of two-layer flows performed by Baines (1979) showed that upstream-moving disturbances generated over bottom topography were especially strong if the speed of the oncoming flow approaches resonance ($\mathrm{Fr} \simeq 1$). At our experiment site, bottom bumps were typically $O(5$ m) in height and $O(50$ m) long (Fig. 2).

Two hours prior to the ISW observation analyzed above, we recorded another energetic internal wave event that had not yet dispersed into solitons. This event was also associated with a Froude number of unity and an elevated b.c. value (Fig. 6).

In the case where the waves are forced locally by flow over a topographic irregularity, the energy transformed into waves traveling along the upstream characteristic will not, on a linear basis, escape from the forcing region when the phase speed c in (19) approaches zero. In this case the forcing will be resonant and the disturbance field will become unbounded on a linear basis. Of course, the wave energy deposited into the downstream characteristic will be propagated away from the source with the Doppler shifted phase speed. This resonantly forced problem has been considered by several authors (e.g., Akylas 1984; Grimshaw and Zeng-

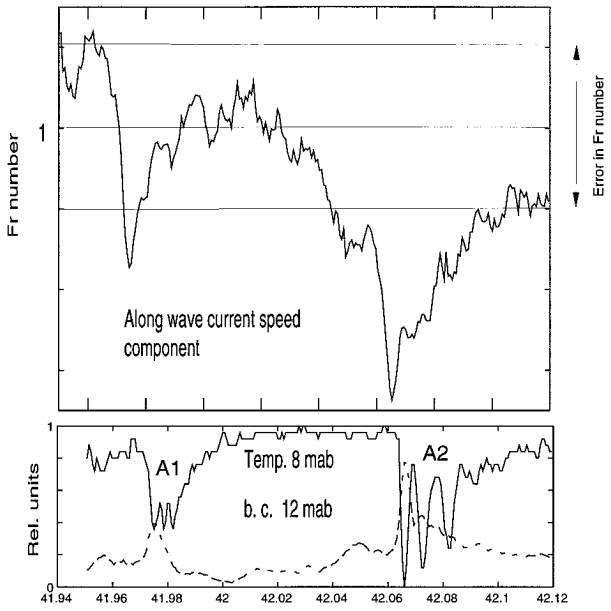

FIG. 11. Time series of the Froude number for two ISW events.

xin 1991) with the result that wave evolution along the (nominally) upstream characteristic is defined by a Korteweg–de Vries equation with a forcing term proportional to the slope of the topographic irregularity. For the purposes of this discussion, we refer to the analysis for resonantly forced internal waves given by Grimshaw and Zengxin (1991) who show, at least for topography of shallow slope, that the response is asymptotically large, $O(\epsilon^{1/2})$, compared to the amplitude of the forcing, $O(\epsilon)$. Some technical difficulties arise, however, when the oncoming flow has velocity shear, but these are described elsewhere (cf. Redekopp 1997, submitted to *J. Fluid Mech.*). Another issue not considered by Grimshaw and Zengxin (1991), but which is important in the context of the present application, pertains to the nonstationarity of the mean flow. This effect was considered by Djordjevic and Redekopp (1992), who showed that a consistent asymptotic approximation for the resonantly forced dynamics was possible when the mean flow varied on a timescale no faster than the wave evolution scale. In this way, the problem of passage through resonance occurring under slowly varying current speeds could be addressed. The final result is that the free-wave evolution equation (19) is modified and, when appropriately scaled, can be rewritten in the form:

$$A_t + \mathcal{U}(t)A_x - \frac{3}{2}AA_x - \frac{1}{6}A_{xxx} = \frac{1}{2}B'(x). \quad (29)$$

The function $\mathcal{U}(t)$ is a scaled departure of the flow speed relative to that for Froude number unity or resonance (i.e., $c = 0$ in the frame of Fig. 12). The right-hand side is the scaled topographic slope [i.e., $B(x)$ is proportional to the amplitude of the topographic deformation].

a. Simulation of ISW generation

The dynamics described by (29) for steady flows consists of a continuous generation of upstream propagating ISWs (e.g., see Grimshaw and Zengxin 1991). Redekopp and You (1995) have examined the forced response described by (29) in the presence of unsteady transcritical flows including the passage through resonance. To simulate the phenomenon described here we have used (29) for the idealized two-layer flow defined by (2) and (3)

Equation (29) was studied numerically for flow over an isolated bump consisting of a Gaussian-shaped deformation of the bottom boundary. Simulations were performed for two different trajectory types of $\mathcal{U}(t)$. These correspond to the observed current variations as shown in Fig. 11 and Fig. 6 (panels A2 and A1).

The first simulation, corresponding to the analyzed ISW wave train, was performed for a case where the current speed relaxed continuously from a supercritical to a subcritical value. The results are shown in Fig. 12. As the current speed passes through the transcritical range, upstream-moving solitons are generated and their number varies proportionally to the residence time of the current in the transcritical range. The solitons are generated in order of decreasing amplitude so no pairwise interactions are possible. As the current speed relaxes further, the entire response reduces to a subcritical lee wave. The lee waves at subcritical speeds can have amplitudes comparable to the lead solitons, but their role in resuspension is expected to be relatively small since they propagate downstream with the current and, therefore, do not have the dramatic interaction with the boundary layer that the upstream-moving solitons have. The observed upstream curvature in the trajectory of the wave crests occurs because the Doppler-shifted wave speed continuously decreases as $\mathcal{U}(t)$ decreases. If the deceleration is strong enough, the initially formed lee waves may eventually propagate upstream over the source. In such circumstances we expect that they will contribute to resuspension similar to the upstream propagating solitons.

The second case, shown in Fig. 13 and which corresponds to another nonlinear event one hour prior to the analyzed ISW (Fig. 6), shows the spatiotemporal response when the oncoming current diminishes quite quickly from a supercritical value into the transcritical range and then accelerates more slowly to a supercritical value again. The upstream portion of the response consists of a packet of three solitons. The trajectory $\mathcal{U}(t)$ is such that the last soliton to be formed has the greatest amplitude (and, therefore, speed) while the first soliton formed has an intermediate amplitude. As a consequence, two pairwise interactions of solitons exist in the proximity of the generating source before the solitons ultimately separate in order of their amplitudes. One suspects that the transient flow field in the boundary layer underneath a pairwise interaction may give rise to stronger resuspension action than under individual solitons in a rank-ordered packet. What is quite astounding, however, is that 73% of the energy in the disturbance field created by this transcritical excursion of the current is transformed into upstream propagating solitons. It is not known whether the fastest moving (i.e., most energetic) or the slowest moving soliton contributes more significantly to resuspension, but their potential as agents for such action exists.

b. Resuspension mechanism: Hypothesis

The square of the local horizontal velocity, which is proportional to the shear stress driving the bottom boundary layer, is shown in Panel D of Fig. 6. During ISW passage the value of u^2 drops to its minimum. This is in contrast to the paradigm that sediment movement and increased particulate loading in the water column are associated with an increase in shear stress, for example, Nittrouer (1994). We propose that this rapid increase in the particulate loading throughout the bottom 12 m is caused by the following process: First, the upstream propagating internal wave generates an (unsteady) adverse pressure gradient (APG) on its leading

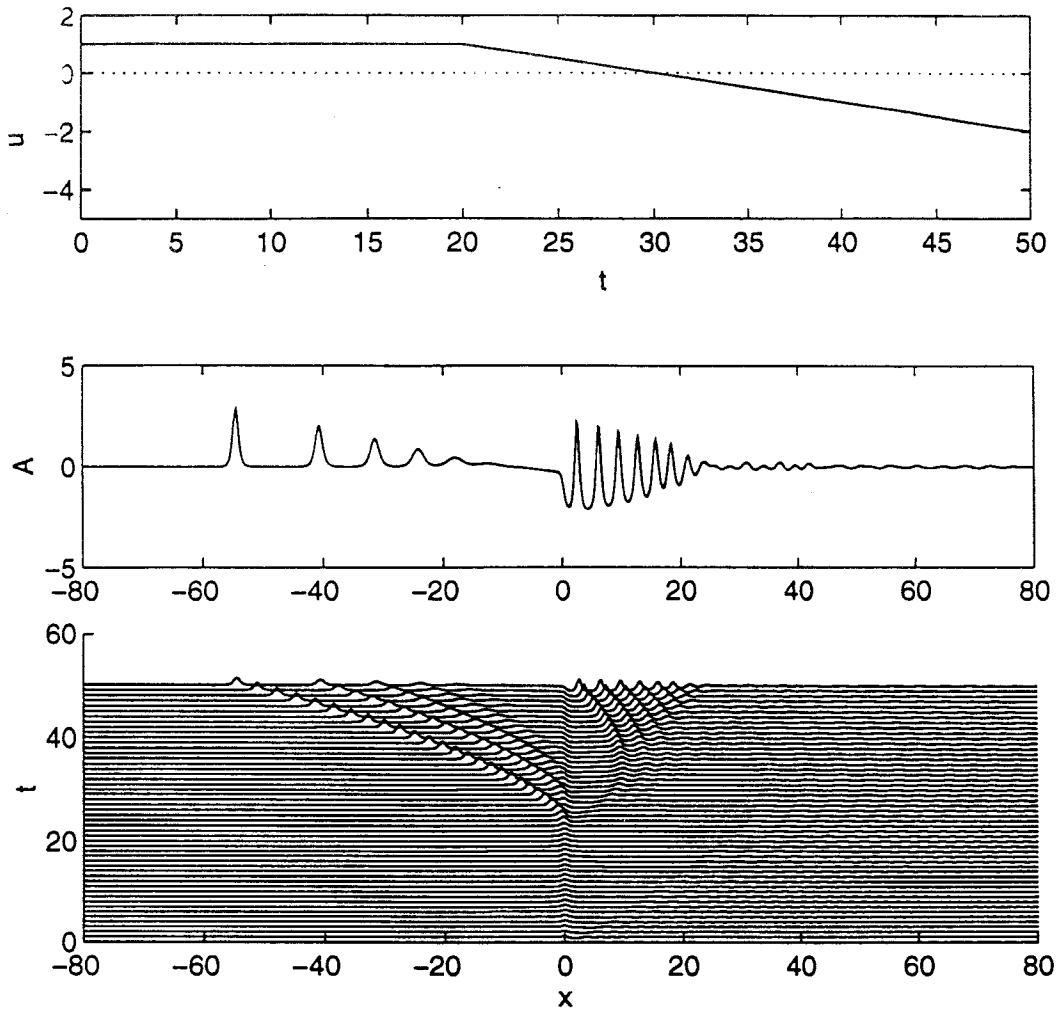

FIG. 12. Numerical solution to the forced KdV equation showing the details of resonant ISW generation. The simulation corresponds to the analyzed case with the current relaxing from super- to subcritical for case A2. The mean current goes from the left to right for this figure. The location of the isopycnal for different times is shown. The bump is placed at $x = 0$. The middle panel shows isopycnal displacement at $t = 50$.

edge. Laboratory experiments (Skare and Krogstad 1994) (steady-state flow study just before flow separation) indicate that the maximum Reynolds stress (which is proportional to the vertical diffusivity) is significantly larger when an APG is observed and is proportional to its magnitude. Second, as the ISW crest approaches the site, the APG is enhanced and becomes so large that the bottom-most part of the flow experiences flow reversal up to 8 m above the bottom (in undisturbed streamline coordinates). The data presented here provide evidence that a sufficiently large upstream propagating ISW wave train behaves like a bottom-layer pump, raising and stirring up the bottom sediment during its passage. This pumping may potentially (for sufficiently large and fast ISWs) lead to sediment transport by mixing upward against the density gradient and into the mixed layer. This is pictorially summarized in Fig. 14. Although we present here only one case of an observed nonlinear internal wave packet, our data record reveals several other events of a similar character (Figs. 5 and 6). Since ISW-like events seem to be frequent features in our observations, and they consistently correspond to elevated values of b.c., we propose that upstream propagating waves not only give rise to favorable conditions for resuspension but may be the major contributors to resuspension. This result implies that resuspension is a spatiotemporal process intimately linked to transcritical current speeds and bottom roughness.

6. Implications for coastal resuspension

We have studied an ISW propagating on the bottom stratified layer and its role in resuspending bottom sediment and mixing it into the water column. We can see from Fig. 5 that resonant ISW generation may have occurred numerous times during the experiment. Gen-

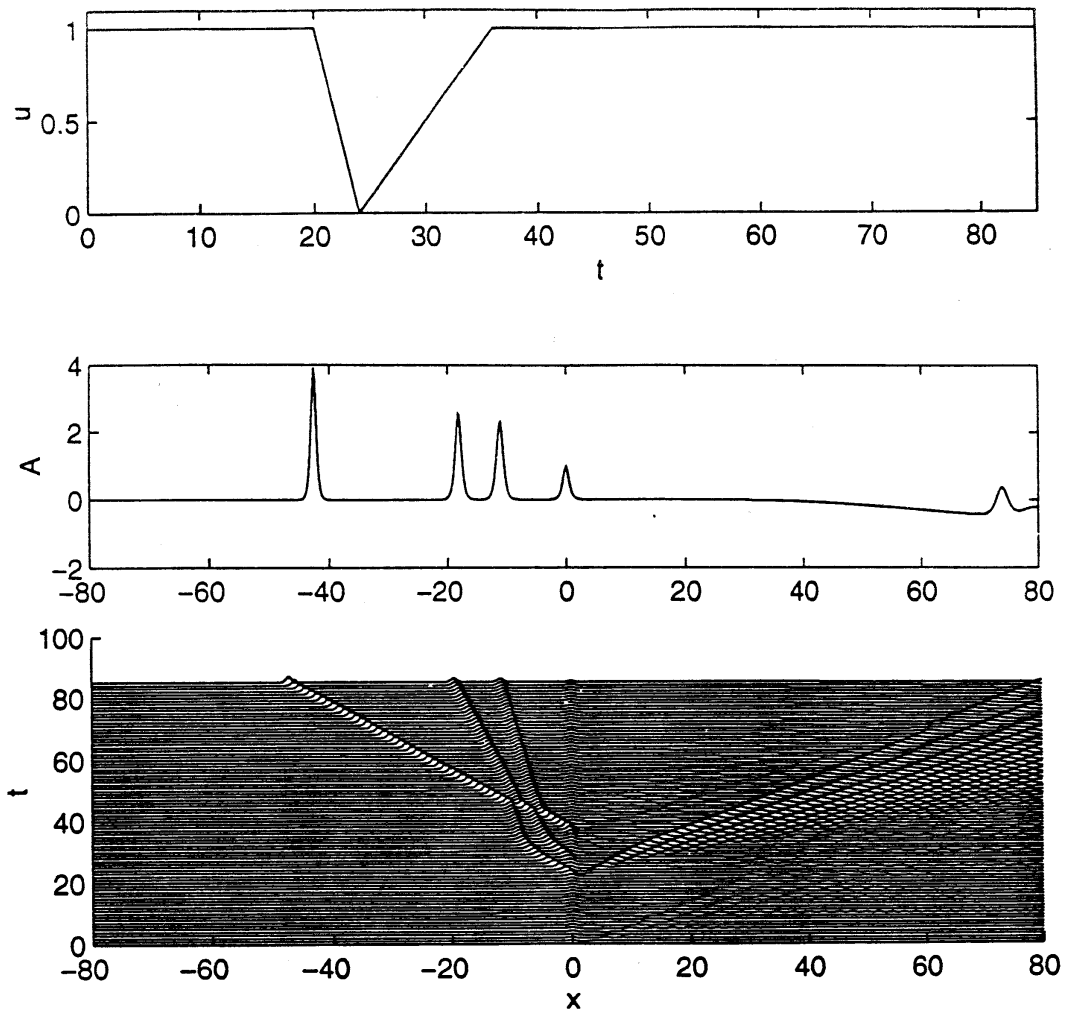

FIG. 13. Numerical solution to the forced KdV equation showing the details of resonant ISW generation for case A1 in Fig. 11.

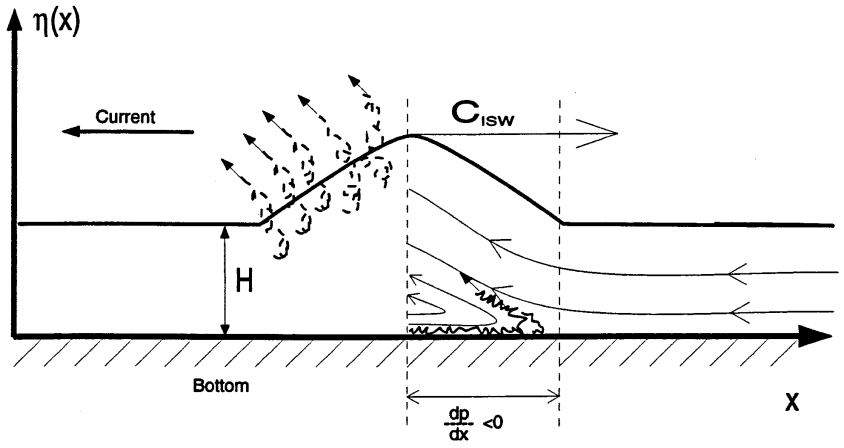

FIG. 14. Schematic representation of ISW action as a bottom-pump. ISW passage stirs sediment up and, for sufficiently large ISWs, transfers bottom material to the unstratified part of the water column.

erally, conditions favorable for ISW generation, and thus of a traveling ''bottom pump,'' occur at our experimental site when the observed stratification coincides with large-scale forcing capable of changing and maintaining the current speed at the bottom (e.g., storms or mesoscale eddies). Since the stratified part of the water column is located at the inner shelf during spring, events such as the one described above are likely to occur on a seasonal basis. The shelf off Palos Verdes appears ideal for resonant ISW generation because the bottom presents a regular scouring pattern perpendicular to the mean flow (Fig. 2). In addition, soliton–soliton interaction may give rise to large intermittent resuspension events in the vicinity of the generating bump while carrying most of the long internal wave field energy.

The present observations have serious implications in the understanding and modeling of sediment resuspension and mixing of bottom material on the continental shelf. The frequent presence of the appropriate stratification [also observed for the SEEP-I experiment site off the U.S. East Coast (Churchill et al. 1994)] and relatively strong alongshore currents provide the necessary ingredients for resonant ISW generation. Despite the short passage time of an ISW, the integrated flux of resuspended matter is a significant part of the total particulate load at the experiment site. Neglecting soliton events would lead to a serious underestimate of sediment resuspension and bottom mixing.

The large vertical diffusivity associated with ISW passage may also have implications on a broader scale (Garrett 1993). Ivey (1987) summarized that mixing at the ocean boundaries may be due to reflection of internal waves or to the interaction of the mean flow with the bottom. This latter process was proposed by Armi (1977) as the source of the enhanced bottom mixing. Resonantly generated ISWs, as presented here, seem to be appropriate mixing agents, as postulated by Armi, since they are continuously generated in the presence of transcritical flow. Thus, resonantly generated ISWs with large induced diffusivity [three orders of magnitude larger than typical values obtained for the ocean interior (Garrett 1993) and of the order required by theory (Armi 1979)] could account for a significant portion of the overall vertical mixing at the ocean bottom.

7. Concluding remarks

Our investigation of the observed upstream propagating ISWs shows that the leading ISW may have triggered bottom-layer separation and/or instability, which was responsible for initiating resuspension under its footprint. We have calculated the ISW-induced Ri to be $O(1/4)$ and on the basis of the beam attenuation record have estimated a vertical eddy diffusivity coefficient K_V to be of order 10^{-2} m^2 s^{-1}. Our observations suggest that ISWs are likely to be generated by transcritical flow over localized irregularities in the bottom topography downstream of the measurement station. These irregularities (scouring) are abundant on the shelf and perpendicular to the mean current. From simulations we have calculated that up to 73% of the energy of the internal wave field can be carried upstream by ISWs. Our observations suggest that resonantly generated ISWs and associated mixing could be important factors in the coastal zone when the internal Froude number is $O(1)$.

Acknowledgments. Vertical hydrographic profiles were kindly provided by Dr. Libe Washburn and Dr. Burt Jones and the high-resolution bottom bathymetry was generously made available by the USGS. We thank Derek Manov for his expertise in developing and deploying the MVMS systems and discussing various problems at different stages of our time series analysis. We thank Dr. D. A. Hammond for executing the forced-KdV simulations and Dr. Mary-Elena Carr for assistance in preparation of the paper. We thank Dr. Murray Levine, Dr. Tony Bowen, and Dr. Ron Zaneveld for helpful discussions. Two anonymous reviewers made comments and suggestions that helped clarify an earlier version. Support was provided by the USC Sea Grant Program and the Office of Naval Research under Grant N00014-96-1-0669 (TD). LGR acknowledges support from the Office of Naval Research under Grant N00014-95-1-0041 and computer support from the San Diego Supercomputer Center.

REFERENCES

Akylas, T. R., 1984: On the excitation of long nonlinear water waves by a moving pressure distribution. *J. Fluid Mech.,* **141,** 455–466.

Armi, L., 1977: The dynamics of the bottom boundary layer of the deep ocean. *Bottom Turbulence,* J. J. Nihoul, Ed., Elsevier, 153–165.

——, 1979: Reply to comments by C. Garrett. *J. Geophys. Res.,* **84,** 5097–5098.

Baines, P. G., 1979: Observations of stratified flow past three-dimensional barriers. *J. Geophys. Res.,* **83,** 7834–7838.

Bender, C. M., and S. A. Orszag, 1978: *Advanced Mathematical Methods for Scientists and Engineers.* McGraw-Hill, 600 pp.

Bogucki, D. J., and C. Garrett, 1993: A simple model for the shear-induced decay of an internal solitary wave. *J. Phys. Oceanogr.,* **23,** 1–10.

Cacchione, D. A., D. E. Drake, J. T. Ferreira, and G. B. Tate, 1994: Bottom stress estimates and sand transport on northern California inner continental shelf. *Contin. Shelf Res.,* **14,** 1273–1289.

Churchill, J. H., P. E. Biscaye, and F. Aikman, 1987: The character and motion of suspended particulate matter over the shelf edge and upper slope off Cape Cod. *Contin. Shelf Res.,* **8,** 789–809.

——, C. D. Wirick, C. N. Flagg, and L. J. Pietrafesa, 1994: Sediment resuspension over the continental shelf east of the Delmarava Peninsula. *Deep-Sea Res.,* **41,** 341–363.

Dickey, T. D., R. H. Douglas, D. Manov, D. Bogucki, P. C. Walker, and P. Petrelis, 1993: An experiment in two-way communication with a multivariable moored system in coastal waters. *J. Atmos. Oceanic Technol.,* **10,** 637–644.

Djordjevic, V. D., and L. G. Redekopp, 1992: Transcritical, shallow-water flow over compact topography. *Wave Motion,* **15,** 1–22.

Eriksen, C. C., 1994: Observations of internal wave reflection and mixing at a seamount. *Proc. Fourth Int. Symp. on Stratified*

Flows, E. Hopfinger, Ed., Institut de Mecanique de Grenoble, 133–151.

Garrett, C., 1979: Mixing in the ocean interior. *Dyn. Atmos.–Oceans*, **3,** 239–265.

——, 1993: A stirring tale of mixing. *Nature*, **364,** 670–671.

Grant, W. D., and O. S. Madsen, 1986: The continental-shelf bottom boundary layer. *Annu. Rev. Fluid Mech.*, **18,** 265–305.

Grimshaw, R., and Y. Zengxin, 1991: Resonant generation of finite-amplitude waves by the flow of a uniformly stratified fluid over topography. *J. Fluid Mech.*, **229,** 603–628.

Hickey, B., 1992: Physical oceanography. *Marine Ecology of the Southern California Bight*, D. Hood, Ed., Pergamon Press, 19–70.

Howell, T. L., and W. S. Brown, 1985: Nonlinear internal waves on the California continental shelf. *J. Geophys. Res.*, **90,** 7256–7264.

Ivey, G. N., 1987: The role of boundary mixing in the deep ocean. *J. Geophys. Res.*, **92,** 11 873–11 878.

Ledwell, J. R., and B. M. Hickey, 1995: Evidence for enhanced boundary mixing in the Santa Monica basin. *J. Geophys. Res.*, **100,** 20 665–20 679.

Levine, M. D., 1981: Dynamic response of the VACM temperature sensor. *Deep-Sea Res.*, **28,** 1401–1408.

Maslowe, S., and L. G. Redekopp, 1980: Long nonlinear waves in stratified shear flows. *J. Fluid Mech.*, **101,** 321–348.

Nichols, M. N., and S. Young, 1991: *The Amazing LA Environment.* Living Planet Press, 145 pp.

Nittrouer, C. A., 1994: Transport of particles across continental shelves. *Rev. Geophys.*, **32,** 85–113.

Ostrovsky, L. A., and Y. A. Stepanyants, 1989: Do internal solitons exist in the ocean? *Rev. Geophys.*, **27,** 293–310.

Redekopp, L. G., and Z. You, 1995: Passage through resonance for the forced Korteweg-deVries equation. *Phys. Rev. Lett.*, **74,** 5158–5161.

Skare, P. E., and P. A. Krogstad, 1994: A turbulent equilibrium boundary layer near separation. *J. Fluid Mech.*, **272,** 319–348.

Spinrad, R. W., H. Glover, B. B. Ward, L. A. Codospoti, and G. Kullenberg, 1989: Suspended particle and bacterial maxima in Peruvian coastal waters during a cold water anomaly. *Deep-Sea Res.*, **36,** 715–733.